LETTERS

Helium solubility in olivine and implications for high $^3He/^4He$ in ocean island basalts

Stephen W. Parman[1]†, Mark D. Kurz[2], Stanley R. Hart[2] & Timothy L. Grove[1]

High $^3He/^4He$ ratios found in ocean island basalts are the main evidence for the existence of an undegassed mantle reservoir[1–3]. However, models of helium isotope evolution depend critically on the chemical behaviour of helium during mantle melting. It is generally assumed that helium is strongly enriched in mantle melts relative to uranium and thorium, yet estimates of helium partitioning in mantle minerals have produced conflicting results[4–6]. Here we present experimental measurements of helium solubility in olivine at atmospheric pressure. Natural and synthetic olivines were equilibrated with a 50% helium atmosphere and analysed by crushing *in vacuo* followed by melting, and yield a minimum olivine–melt partition coefficient of 0.0025 ± 0.0005 (s.d.) and a maximum of 0.0060 ± 0.0007 (s.d.). The results indicate that helium might be more compatible than uranium and thorium during mantle melting and that high $^3He/^4He$ ratios can be preserved in depleted residues of melting. A depleted source for high $^3He/^4He$ ocean island basalts would resolve the apparent discrepancy[7] in the relative helium concentrations of ocean island and mid-ocean-ridge basalts.

Although there is a general consensus that Earth started with an initial $^3He/^4He$ ratio of $\sim 120R_a$ ($R_a = (^3He/^4He)_{sample}/(^3He/^4He)_{atmosphere}$), its subsequent evolution is not well constrained[8]. In the 'standard' model, He is assumed to be more incompatible than U + Th (the parent isotopes of ^4He) during melting[9]. If so, any melting event will leave the mantle residue enriched in U + Th relative to He, and it will evolve radiogenic He isotope ratios (low $^3He/^4He$; Fig. 1a). In this model, the unmelted, undegassed mantle has the highest $^3He/^4He$ ratios and highest He concentrations of any mantle reservoir and is the likely source of high $^3He/^4He$ in ocean island basalt (OIB)[2,9].

In an alternative model, He is assumed to be more compatible than U + Th during melting, in which case melting decreases the parent/daughter ratio (U + Th)/He of the mantle. Therefore the $^3He/^4He$ ratio of a depleted residue will decrease more slowly with time than an undegassed reservoir (Fig. 1b). In this case, the highest $^3He/^4He$ mantle reservoirs are the depleted residues of melting, but unlike in the standard model, these high $^3He/^4He$ sources will have low He concentrations[10]. The older the depletion event and the greater the degree of melting, the larger the difference will be between a depleted and undepleted source.

Most OIBs have higher $^3He/^4He$ ratios and lower gas contents than mid-ocean-ridge basalt (MORB)[11–13]. This has been termed the 'helium paradox'[7] and is more consistent with the alternative model than the standard model. However, concentrations of noble gases in lavas are dominated by shallow degassing processes, and the relative gas concentrations in OIBs and MORBs may not reflect the gas concentrations in their sources. Studies of concentration ratios (for example He/Ne) indicate that simple degassing cannot explain

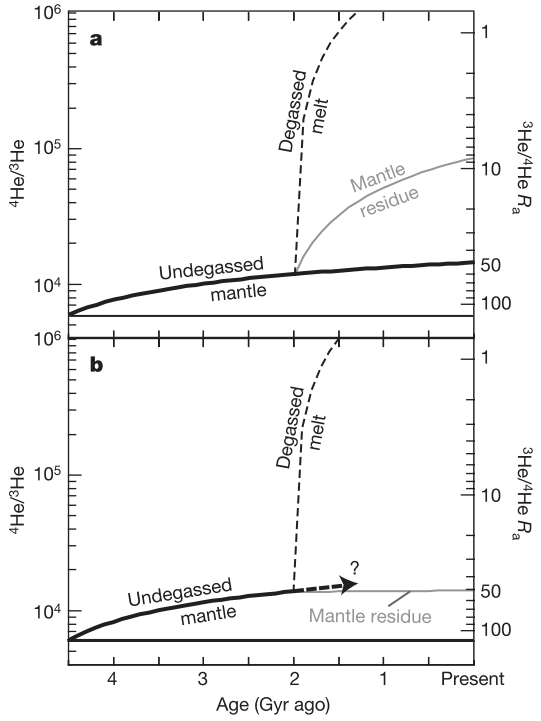

Figure 1 | Age versus He isotope ratios for two different helium isotopic evolution models. Both start with an initial $^3He/^4He$ of $120R_a$ (ref. 8). **a**, The standard model, in which helium is more incompatible than U and Th. The undegassed mantle (thick black line, $(^{238}U/^3He)_{present} = 450$, $(^{232}Th/^{238}U)_{present} = 4$) is assumed to be sampled by OIB and so the model parameters are set to produce a $^3He/^4He$ ratio of 50 (the highest measured $^3He/^4He$ in OIB[30]) in the undegassed mantle. A melting event at 2 Gyr is also shown, at which point the $(^{238}U/^3He)$ of the depleted mantle is increased by a factor of 28.6 relative to the undegassed mantle, such that it evolves to a present-day value of $8R_a$ (grey line). This is one model for the origin of the depleted MORB source. The melt has a low (U+Th)/He until it approaches the surface and degasses, increasing the $(^{238}U/^3He)$ 1,000-fold. Oceanic and crustal materials made from such degassed melts will rapidly evolve very low $^3He/^4He$ ratios (dashed line). The horizontal line shows a constant $^3He/^4He$ for reference. **b**, Alternative model in which He is more compatible than U+Th (the line styles are the same as in **a**). Here we assume that the highest $^3He/^4He$ OIBs are melts of depleted mantle. The undegassed mantle has $(^{238}U/^3He)_{present} = 600$ and $(^{232}Th/^{238}U)_{present} = 4$, and melting at 2 Gyr produces a depleted residue with a $(^{238}U/^3He)$ one-tenth that of the undegassed mantle, which evolves to a present-day $^3He/^4He$ of 50. As in **a**, the degassed melt rapidly evolves low $^3He/^4He$.

[1]Department of Earth, Atmospheric and Planetary Sciences, Massachusetts Institute of Technology, Building 54, Cambridge, Massachusetts 02139, USA. [2]Woods Hole Oceanographic Institute, Clark Building, Woods Hole, Massachusetts 02543, USA. †Present address: Department of Earth Sciences, University of Durham, Science Labs, Durham DH1 3LE, UK.

the differences in noble-gas concentrations or their relative abundances in most cases. A variety of more complex degassing models have been proposed to resolve the helium paradox within the framework of the standard model[11,12,14]. Nevertheless, no direct observation indicates that the OIB source is gas-rich compared with the MORB source, as required by the standard model.

To help in distinguishing between the two models, we have measured the solubility of He in natural and synthetic olivine by using high-temperature controlled-oxygen-fugacity experiments at 1 atm pressure. The experiments were specifically designed to avoid the entrapment of melt or gas inclusions, problems that affected previous experimental studies[4,5,15] (Fig. 2; see Methods). In particular, the olivine samples were not placed in contact with a melt phase. The partition coefficient of helium (D^{He}) between olivine and melt is calculated from the published solubility of He in basaltic melts[16,17]. The melts used in those studies were close to (although not exactly in) equilibrium with the olivines used in our experiments. The errors introduced into our calculation of D should be negligible, because He solubility seems to vary little in basaltic compositions[16,17].

He concentrations in the experimental olivines were measured by noble-gas mass spectrometry by crushing *in vacuo* followed by melting of the crushed sample[18]. Crushing is thought to release only gas trapped in melt and gas inclusions, whereas subsequent melting releases the gas dissolved in the crystal structure. However, 50–70% of the total gas contained in our samples was released by crushing (Fig. 3). On the basis of extensive microscopic examination of the starting materials and run products, we believe that this was not caused by gas inclusions, bubbles or nanopores (see Methods). Moreover, both natural and synthetic olivine samples yielded the same gas release pattern (Fig. 3). If inclusions were dominating the He release this should not occur, because the two types of olivine should have very different inclusion populations. This indicates that some of the gas released during crushing might actually be dissolved in the olivine structure, as has been observed in some previous studies[19]. However, this evidence is circumstantial. Nanometre-scale inclusions or voids cannot be completely ruled out as a source for the crush gas at this point.

Three additional experiments were performed in which the olivine starting material was ground to submillimetre grain sizes before the experiment, to test the influence of sintering and surface area. These samples showed slightly elevated gas release during both crushing and melting (Fig. 3), indicating that measurable quantities of gas can be trapped between grains or adsorbed on grain surfaces. This is probably the cause of high values of D for noble gases in previous studies that used fine (<10-μm diameter) mineral powders[15]. However, the results show that, in the present experiments, sintering and surface adsorption were not major sources of He.

The amount of gas released by melting of the crushed powders was quite consistent, yielding a D^{He} of 0.0025 ± 0.0005 (excluding experiment 106C, see Fig. 3 caption and Methods). The similarity of D^{He} in natural, iron-bearing and synthetic, iron-free olivine indicates that vacancies might have a limited effect on He solubility because the point-defect population in olivine is primarily controlled

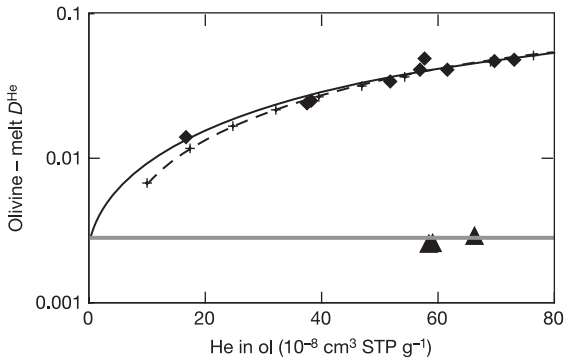

Figure 2 | Plot of helium content of experimental olivines against the calculated olivine–melt D^{He} for the data of ref. 4 (filled diamonds) and the present study (filled triangles). The data from ref. 4 show a large range of D^{He} that correlates with the He contents of the olivines. A true partition coefficient is expected to obey Henry's law and should be constant (grey horizontal line). A model in which an olivine with low He contents (10^{-7} cm^3 STP g^{-1}) is variably contaminated with the melt from the experiments fits the data very well (dashed curve) and indicates that melt inclusions in the olivine might be responsible for the changing D values and He contents in ref. 4. A linear fit (representing a mixing line) through the data (solid black curve) yields an R^2 of 0.951 and an intercept of 0.0027. The intercept represents the D^{He} value at a hypothetical zero level of contamination and is a lower limit on D^{He} in the experiments of ref. 4. The lower limit corresponds well to the D^{He} values (0.0025–0.0060) reported here and indicates that the experiments might be obeying Henry's law. The D values of this study were calculated by dividing the amount of He released by melting by the solubility of He in basaltic melt (5×10^{-4} cm^3 STP g^{-1} atm^{-1})[16,17].

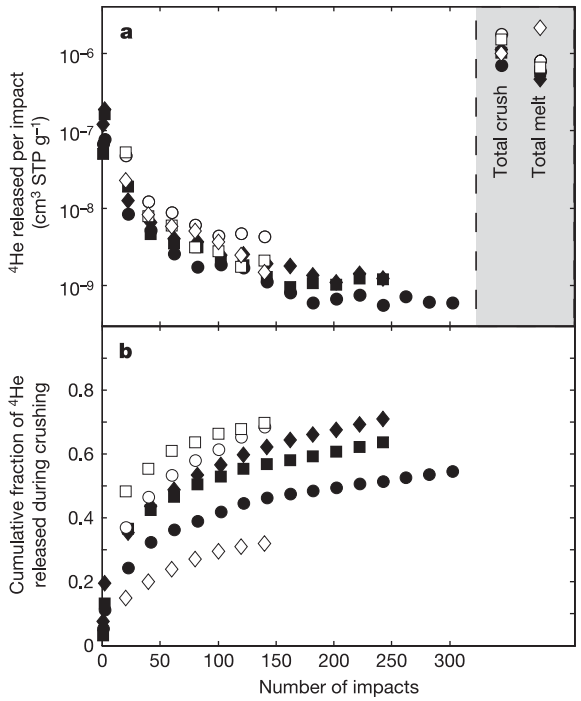

Figure 3 | Helium released from experimental olivine grains during crushing and melting. a, Gas released per impact. For the large-grain-size experiments 100A (filled circles, AAA gem San Carlos olivine), 102A (filled squares, AA gem San Carlos olivine) and 104A (filled diamonds, pure synthetic forsterite) and for the powder experiments 106A (open circles, <100-μm grains, San Carlos olivine), 106B (open squares, ~750-μm grains, San Carlos olivine) and 106C (open diamonds, ~500-μm grains, San Carlos olivine). The values for gas released are calculated by dividing the amount of gas measured at each analytical step by the number of impacts that occurred since the last analysis and therefore represent average release values over that span of impacts. The last two symbols in each sequence (in the grey region) are the total amount of gas released by crushing and by melting. Excluding experiment 106C, the total amount of gas released by crushing is more variable (RSD = 34%) than the amount released by melting (RSD = 21%), indicating that some part of the crush gas might reside in a different location than the gas released by melting. **b**, Cumulative amount of gas released by crushing divided by the total amount of gas released. The symbols are the same as in **a**. Between 50% and 70% of the total (crush+melt) gas in the samples is released by crushing (excluding experiment 106C). The gas release curves flatten after ~150 impacts, indicating either that there might be some fraction (~20%) of the gas that cannot be released by crushing or that the crushing process might have reached its limit and is no longer breaking grains.

by Fe^{3+} substitutions[20]. For the same reason, the effect of oxygen fugacity f_{O_2} on D^{He} should also be relatively small. The total amount of He released by crushing and melting (using only the large-grain-size experiments) yields an average D^{He} of 0.0060 ± 0.0007, the maximum value that these experiments would support. Because we do not fully understand the origin of the gas released by crushing, in the following discussion we use only the lower value of 0.0025. Using the higher value would only strengthen our conclusions. This value is lower than previous experimental measurements (0.01–0.005)[4,5] and within estimates of maximum D^{He} based on natural olivine–melt pairs: 0.001 (M.D.K., unpublished observations) to 0.008 (ref. 6). Note that our value for D^{He} is, strictly, valid only at the experimental conditions. We assume that D^{He} is similar at mantle melting conditions. Preliminary experiments on the effects of oxygen fugacity and temperature support this view, although the effects of pressure have yet to be quantified.

The solubility experiments indicate that ancient melt-depleted mantle might retain high $^3He/^4He$ ratios. D^{He} in olivine (ol) is similar to the estimated D^{He} for clinopyroxene (cpx)[21], indicating that He might be distributed relatively evenly between the mantle minerals (Fig. 4). In contrast, most trace elements (including U and Th) are strongly concentrated in cpx and garnet (gt). Thus, unlike other isotopic systems (for example Sr, Nd and Pb), the parent isotopes ($^{235,238}U$ and ^{232}Th) in the He system may reside largely in a different mantle mineral from their daughter isotope (^4He). This has implications for He isotope evolution because mantle melting is non-modal. That is, the minerals do not enter the melt in the same proportion in which they are present in the mantle. Clinopyroxene and gt enter the melt at 2-3 times the rate of ol and orthopyroxene (opx)[22]. So, as melting proceeds, the fraction of cpx and gt (the main carriers of the parent isotopes) in the residue will decrease and the fraction of ol (the main carrier of the daughter isotope) will increase.

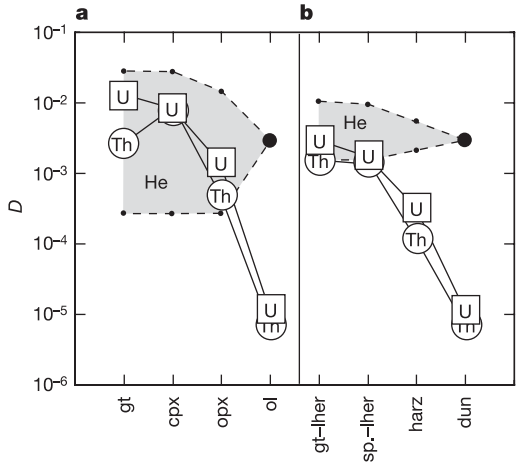

Figure 4 | Partition coefficients for U (squares), Th (circles) and He (filled circles and field) relevant to mantle melting. a, Individual mineral–melt *D* values for garnet (gt), clinopyroxene (cpx), orthopyroxene (opx) and olivine (ol). **b**, Bulk *D* values for garnet lherzolite (gt–lher), spinel lherzolite (sp–lher), harzburgite (harz) and dunite (dun). The D^{He} value for olivine is from this study (large filled circle). We assume that the value measured at 1 atm is applicable to melting at depth. Values for D^{He} in gt, cpx and opx have not been published. Here we use experiments on the heavier noble gases[21] and He analyses from natural samples[28] to infer upper and lower bounds on D^{He} in these minerals. Partition coefficients for U and Th are averages of all published values. No partitioning data are available for spinel and so all *D* values are assumed to be zero. See Methods for a full discussion of how the *D* values were calculated and for the references used. During the early stages of melting (lherzolite assemblage), the bulk *D* for U and Th fall on the lower side of the D^{He} field. However, the bulk *D* for U and Th quickly decrease as melting proceeds and the residue approaches harzburgite (ol + opx) and dunite (ol) assemblages. The fractions of minerals [ol, opx, cpx, sp, gt] used in the calculation of the bulk *D* values are garnet lherzolite [0.61, 0.13, 0.13, 0.0, 0.13], spinel lherzolite [0.61, 0.20, 0.17, 0.02, 0.0], harzburgite [0.74, 0.23, 0.0, 0.03, 0] and dunite [1.0, 0, 0, 0, 0].

During early melting of a gt or spinel (sp) lherzolite (ol+opx+cpx+sp/gt), the bulk *D* (the mineral–melt *D* values multiplied by their modal fraction in the mantle) for U and Th may be close to that of He, but will rapidly fall as cpx and gt are removed by non-modal melting (Fig. 4). In contrast, the bulk *D* for He will remain relatively constant or may even rise. When all of the cpx and gt are removed, leaving a harzburgite residue, D^{U+Th} will be significantly lower than D^{He} (Fig. 4). For dunite, the difference will be even greater. Harzburgite and especially dunite residues should have exceedingly low (U + Th)/He, and will preserve high $^3He/^4He$ ratios relative to an undegassed source (Fig. 1b).

Given the paucity of noble-gas partitioning data, quantitative modelling assuming a particular melting style (for example batch, fractional or continuous) is premature. However, a few points can be made. If the bulk *D* for He is greater than the bulk *D* for U+Th, then both batch and fractional models will produce residues with low (U+Th)/He. Fractional melting will produce the most fractionated (lowest) (U+Th)/He, whereas batch melting will produce the least. Other melting models will fall between these two extreme cases. Combined with the effects of non-modal melting, the difference between D^{He} and D^{U+Th} in olivine is so large that it eclipses most other factors (Fig. 4).

Whereas our experimental samples were specifically chosen for their lack of mineral, melt or gas inclusions, most natural minerals have such inclusions. Melt inclusions will act as phases with $D = 1$ for all elements. Gas inclusions will have high *D* for helium but low *D* for U and Th. Thus, the effective olivine–melt D^{He} in nature is likely to be higher than our measured value on 'unnaturally' inclusion-free minerals.

It is likely that depleted residues are present throughout the mantle. Clinopyroxene-poor lherzolites, harzburgites and dunites are produced at mid-ocean ridges[23] and subduction zones[24], and are subducted at convergent margins. In addition, ^{142}Nd isotope data indicate that most of the mantle might have been depleted early in Earth's history[25]. If depleted residues can retain high $^3He/^4He$, they are potential sources for at least some of the high-$^3He/^4He$ OIB. Correlations between Sr, Nd and He isotopes have been used to support this idea[26]. However, undegassed mantle can also yield high $^3He/^4He$ in OIB (Fig. 4). The most direct way to distinguish between the two possibilities would be to accurately constrain the pre-degassing abundances of He and other noble gases in OIB and MORB. The low He concentrations in OIB, relative to MORB, indicate that they might have ancient depleted sources, but confirming this hypothesis will require significant advances in our understanding of magmatic devolatilization mechanisms and volatile element fractionation.

METHODS

Experiments. To avoid the problems encountered in previous studies, the olivine samples were equilibrated directly with a 50% (v/v) He atmosphere in a 1-atm gas mixing furnace at 1,350 °C. The remaining 50% of the atmosphere was a mixture of CO_2 and H_2, which was used to maintain the f_{O_2} at the Ni–NiO oxygen buffer. The samples were large (millimetre-sized) pieces of inclusion-free, gem-quality olivine. These were placed in large (centimetre-sized) capsules of San Carlos olivine and run for 17–21 days to ensure diffusive equilibrium[27]. There was no evidence of sintering or reaction after the experiment. Three starting materials were used: two types of natural San Carlos olivine (AAA and AA grade, faceted gems) and a synthetic pure forsterite (produced by the Linde Corporation). The starting materials for experiment 100A were extensively examined for inclusions and pores before and after the experiments, by optical microscopy, back-scattered and secondary electron imaging, and annular dark-field/bright-field imaging with a scanning transmission electron microscope (STEM). The materials were inclusion-free and pore-free down to the resolution of the STEM, ~10 nm. The volume of olivine imaged with the STEM was $\sim 10^9$ nm^3.

Three additional experiments were performed in which the starting material (non-gem-quality San Carlos olivine) was ground to <100-μm, ~500-μm and ~750-μm grain size to examine the effects of surface area and sintering. Other than the grain size, the experimental conditions were the same as for the first three experiments. The materials in run 106A, with the <100-μm grain size, sintered together and to the capsule wall, whereas those in the other two powder experiments did not. Run conditions and analytical data are provided in Supplementary Tables 1 and 2.

Gas analyses. For the large-grain-size experiments, the analyses were performed after every 20 impacts except for the first two analyses, which were taken after one impact. For the powdered experiments, analyses were taken after every 20 steps. The large-grain-size experiments (100A, 102A and 104A) show highly consistent crushing (total crush relative standard deviation (RSD) = 23%) and melting (melt RSD = 14%) release patterns. The powder experiments (106A, 106B and 106C) show noticeably higher gas release during crushing and melting. Experiment 106C in particular is anomalous with large amounts of gas released during melting and small amounts of gas released during crushing relative to the other powdered experiments. This experiment is excluded from all calculations of solubility and partitioning. Considering all of the experiments except 106C, the total amount of gas released by crushing is more variable (RSD = 34%) than the amount released by melting (RSD = 21%), indicating that some part of the crush gas might reside in a different location from the gas released by melting.

Partition coefficients. The grey field in Fig. 4 represents the range of He D values that can be supported by experimental or, lacking that, natural estimates of partition coefficients. The lower bounds on D^{He} in gt, cpx and opx are based on the published experimental D values for Ne, Ar, Kr and Xe in cpx[21]. We extrapolated the lattice-strain parabola for cpx defined by the noble gases heavier than He, which yields a value of ~0.0003. As there are no noble-gas partitioning data for opx or gt we make the *ad hoc* assumption that they have the same D^{He} as cpx. The upper bound was estimated from measurements of total He contents in ol, opx and cpx in peridotites[28]. The data are quite scattered, with relative standard deviations up to 100%. From median values, the opx has about fivefold more He, and the cpx about tenfold more He, than the olivine crystals in the samples. For the upper curve we assume that these ratios also reflect the relative sizes of the partition coefficients. As there are no gt data for the peridotite, we assume that its D^{He} is the same as that for cpx. The peridotite data are strongly affected by inclusions, but they do indicate a plausible upper bound. The decrease in D^{He} from cpx to opx to ol in the natural data resembles the decreasing compatibility of other incompatible trace elements (for example U and Th) in these minerals (Fig. 4), and would be consistent with He partitioning being controlled by the same parameters (for example atomic size, charge and lattice-site size mismatch) that control most trace element partitioning[21].

The mineral–melt D values for U and Th are averages of published experimental data (references in Supplementary Information). Our bulk D values calculated from the average mineral–melt D values (Fig. 4) agree well with bulk D values calculated from lattice-strain models[29].

Received 12 April; accepted 2 September 2005.

1. Kurz, M. D., Jenkins, W. J. & Hart, S. R. Helium isotopic systematics of oceanic islands and mantle heterogeneity. *Nature* **297,** 43–47 (1982).
2. Moreira, M., Doucet, S., Madureira, P. M., Lecomte, A. & Allègre, C. J. Helium-neon systematics in OIB and the nature of the source of mantle plumes. *Geochim. Cosmochim. Acta* **68,** A283 (2004).
3. Allegre, C. J., Staudacher, T., Sarda, P. & Kurz, M. Constraints on the evolution of the Earth's mantle from rare-gas systematics. *Nature* **303,** 762–766 (1983).
4. Hiyagon, H. & Ozima, M. Partition of noble-gases between olivine and basalt melt. *Geochim. Cosmochim. Acta* **50,** 2045–2057 (1986).
5. Brooker, R. A., Heber, V., Kelley, S. P. & Wood, B. J. Noble gas partitioning behaviour during mantle melting: a possible explanation for 'the He paradox'? *EOS* **84,** Abstract V31F–03 (2003).
6. Marty, B. & Lussiez, P. Constraints on rare-gas partition-coefficients from analysis of olivine glass from a picritic midocean ridge basalt. *Chem. Geol.* **106,** 1–7 (1993).
7. Anderson, D. L. The helium paradoxes. *Proc. Natl Acad. Sci. USA* **95,** 4822–4827 (1998).
8. Graham, D. W. in *Noble Gases in Geochemistry and Cosmochemistry* (eds Porcelli, D., Ballentine, C. J. & Wieler, R.) 247–317 (The Mineralogical Society of America, Washington DC, 2002).
9. Kurz, M. D. Mantle heterogeneity beneath oceanic islands—some inferences from isotopes. *Phil. Trans. R. Soc. Lond. A* **342,** 91–103 (1993).
10. Meibom, A. *et al.* Are high He-3/He-4 ratios in oceanic basalts an indicator of deep-mantle plume components? *Earth Planet. Sci. Lett.* **208,** 197–204 (2003).
11. Yamamato, J. & Burnard, P. G. Solubility controlled noble gas fractionation during magmatic degassing: implications for noble gas compositions of primary melts of OIB and MORB. *Geochim. Cosmochim. Acta* **69,** 727–734 (2005).
12. Honda, M. & Patterson, D. B. Systematic elemental fractionation of mantle-derived helium, neon, and argon in mid-oceanic ridge glasses. *Geochim. Cosmochim. Acta* **63,** 2863–2874 (1999).
13. Workman, R. K. *et al.* Recycled metasomatized lithosphere as the origin of the enriched mantle II (EM2) end-member: evidence from the Samoan volcanic chain. *Geochem. Geophys. Geosyst.* **5,** doi:10.1029/2003GC000623 (2004).
14. Burnard, P. G., Graham, D. W. & Farley, K. A. Mechanisms of magmatic gas loss along the Southeast Indian Ridge and the Amsterdam–St. Paul Plateau. *Earth Planet. Sci. Lett.* **203,** 131–148 (2002).
15. Broadhurst, C. L., Drake, M. J., Hagee, B. E. & Bernatowicz, T. J. Solubility and Partitioning of Ne, Ar, Kr, and Xe in minerals and synthetic basaltic melts. *Geochim. Cosmochim. Acta* **56,** 709–723 (1992).
16. Lux, G. The behaviour of noble-gases in silicate liquids—solution, diffusion, bubbles and surface effects, with applications to natural samples. *Geochim. Cosmochim. Acta* **51,** 1549–1560 (1987).
17. Jambon, A., Weber, H. & Braun, O. Solubility of He, Ne, Ar, Kr and Xe in a basalt melt in the range 1250–1600 degrees C. *Geochim. Cosmochim. Acta* **50,** 401–408 (1986).
18. Kurz, M. D., Curtice, J., Lott, D. E. & Solow, A. Rapid helium isotopic variability in Mauna Kea shield lavas from the Hawaiian Scientific Drilling Project. *Geochem. Geophys. Geosyst.* **5,** doi:10.1029/2002GC000439 (2004).
19. Yokochi, R., Marty, B., Pik, R. & Burnard, P. High $^3He/^4He$ ratios in peridotite xenoliths from SW Japan revisited: Evidence for cosmogenic ^3He released by vacuum crushing. *Geochem. Geophys. Geosyst.* **6,** doi:10.1029/2004GC000836 (2005).
20. Nakamura, A. & Schmalzried, H. On the nonstoichiometry and point-defects of olivine. *Phys. Chem. Miner.* **10,** 27–37 (1983).
21. Brooker, R. A. *et al.* The 'zero charge' partitioning behaviour of noble gases during mantle melting. *Nature* **423,** 738–741 (2003).
22. Baker, M. B. & Stolper, E. M. Determining the composition of high-pressure mantle melts using diamond aggregates. *Geochim. Cosmochim. Acta* **58,** 2811–2827 (1994).
23. Dick, H. J. B., Fisher, R. L. & Bryan, W. B. Mineralogic variability of the uppermost mantle along mid-ocean ridges. *Earth Planet. Sci. Lett.* **69,** 88–106 (1984).
24. Gill, J. B. *Orogenic Andesites and Plate Tectonics* (Springer, New York, 1981).
25. Boyet, M. & Carlson, R. W. ^{142}Nd evidence for early (>4.53 Ga) global differentiation of the Silicate Earth. *Science* (in the press) (2005).
26. Class, C. & Goldstein, S. L. Evolution of helium isotopes in the Earth's mantle. *Nature* **436,** 1107–1112 (2005).
27. Trull, T. W. & Kurz, M. D. Experimental measurements of He-3 and He-4 mobility in olivine and clinopyroxene at magmatic temperatures. *Geochim. Cosmochim. Acta* **57,** 1313–1324 (1993).
28. Dunai, T. J. & Baur, H. Helium, neon, and argon systematics of the European subcontinental mantle—implications for its geochemical evolution. *Geochim. Cosmochim. Acta* **59,** 2767–2783 (1995).
29. Landwehr, D., Blundy, J., Chamorro-Perez, E. M., Hill, E. & Wood, B. U-series disequilibria generated by partial melting of spinel lherzolite. *Earth Planet. Sci. Lett.* **188,** 329–348 (2001).
30. Stuart, F. M., Lass-Evans, S., Fitton, J. G. & Ellam, R. M. High $^3He/^4He$ ratios in picritic basalts from Baffin Island and the role of a mixed reservoir in mantle plumes. *Nature* **424,** 57–59 (2003).

Supplementary Information is linked to the online version of the paper at www.nature.com/nature.

Acknowledgements We thank J. Curtice for his long labours with the He analyses, and J. van Orman for assistance in the early planning and execution of the project. This research was supported by the NSF.

Author Contributions S.W.P. and T.L.G. performed the experiments and microscopic observations. M.D.K. performed the He analysis. S.R.H. contributed to experimental and analytical design. All authors contributed to data analysis.

Author Information Reprints and permissions information is available at npg.nature.com/reprintsandpermissions. The authors declare no competing financial interests. Correspondence and requests for materials should be addressed to S.W.P. (stephen.parman@durham.ac.uk).